Chemical Engineering Science 330 (2026) 123910

Contents lists available at ScienceDirect

Chemical Engineering Science

journal homepage: www.elsevier.com/locate/ces

One-pot/solvent-free aerobic oxidation of KA oil to ε-caprolactone catalyzed by carbon nanotubes: Integrated alcohol-to-ester pathway, kinetic modeling and economic evaluation

Zhangzhi Li [a,1], Yelin Guan [a,1], Zhihui Cai [a], JieFeng Zhou [a], Hongjuan Wang [a], Hao-Fan Wang [a], Shuang Li [b], Yonghai Cao [a,*], Hao Yu [a]

[a] School of Chemistry and Chemical Engineering, Guangdong Provincial Key Lab of Green Chemical Product Technology, South China University of Technology, Guangzhou 510641, China
[b] School of Biology and Biological Engineering, South China University of Technology, Guangzhou 510006, China

ARTICLE INFO

Keywords:
KA oil
Carbon nanotubes
N doping
ε-Caprolactone
Kinetic model

ABSTRACT

KA oil (a mixture of cyclohexanone (Cy=O) and cyclohexanol (Cy-OH)) was directly used as a drop-in replacement for Cy=O in the synthesis of ε-caprolactone (ε-CL), eliminating any pre-separation or purification step and providing a highly efficient, low-cost route with considerable scale-up potential. Metal-free nitrogen-doped carbon nanotubes (NCNTs) were employed as the catalyst, and O_2/benzaldehyde (BZA) acted as the cooperative oxidant for the aerobic oxidation of KA oil to ε-CL. Under optimized conditions, NCNTs afforded 19.68 % conversion of KA oil, 93.27 % selectivity to ε-CL, 0.37 of aldehyde efficiency (AE), and 41.93 g h^{-1} L^{-1} of space–time yield (STY), all exceeding the performance of undoped catalysts or blank runs. The high K/A ratio (2.00) revealed that N doping could greatly enhance the alcohol-to-ester pathway, while ketones acted as key intermediates. Detailed mechanistic studies revealed that N doping simultaneously accelerated the alcohol-to-ketone and ketone-to-ester steps, an effect most pronounced at low temperature, and concomitantly lowered the apparent activation energy. Structure–activity correlations identified graphitic (N_G) and pyridinic nitrogen (N_P) as the critical active sites, whereas surface oxygenated functionalities suppressed side reactions and enhanced AE. Kinetic analysis delivered reaction orders and rate constants for the three dominant pathways, and established a predictive kinetic model, which confirmed that N incorporation reduced the activation energy, and elevated both the rates and the effective reaction orders of all three steps. The full-flowsheet economic simulation and Life Cycle Assessment (LCA) analysis demonstrated the robust economic attractiveness and low the energy consumption of the proposed process.

1. Introduction

ε-Caprolactone (ε-CL) serves as a pivotal platform chemical across industry, most notably as the monomer for biodegradable poly(ε-caprolactone) (Gross and Kalra, 2002). Generally, ε-CL is traditionally produced via the typical Baeyer-Villiger (BV) oxidation of cyclohexanone (Cy=O) with stoichiometric oxidants such as peracids or H_2O_2 (Jiménez-Sanchidrián and Ruiz, 2008), which suffers from high cost and severe safety issues (ten Brink et al., 2004; Wang et al., 2023). Recently, a greener protocol employing O_2/aldehyde as a sacrificial co-oxidant avoiding peroxides was proposed (Nabae et al., 2013). In this process, aromatic or aliphatic aldehydes are used to react with O_2 to generate peroxy species, which subsequently oxidize Cy=O to ε-CL (Huang et al., 2026; Nabae et al., 2013; Zhang et al., 2019). Nevertheless, this route still faces two tough issues: (i) raw Cy=O is always co-produced with cyclohexanol (Cy-OH), and the purification step markedly increases the process cost; (ii) the strongly exothermic oxidation requires large amounts of solvent, lowering the production capacity.

'Cy=O is manufactured commercially by the liquid-phase oxidation of cyclohexane or by hydrogenation of phenol (Fig. 1), both of which afford a Cy=O/Cy-OH mixture (KA oil). To obtain pure Cy=O, Cy-OH must be separated or further dehydrogenated, entailing additional

* Corresponding author.
E-mail address: meyhcao@scut.edu.cn (Y. Cao).
[1] These authors contributed equally.

https://doi.org/10.1016/j.ces.2026.123910
Received 3 January 2026; Received in revised form 23 March 2026; Accepted 30 March 2026
Available online 1 April 2026
0009-2509/© 2026 Elsevier Ltd. All rights are reserved, including those for text and data mining, AI training, and similar technologies.

energy input (Bellomi et al., 2023). Direct conversion of KA oil to ε-CL would therefore eliminate the purification penalty and significantly improve process economics (Du et al., 2019). However, alcohols are efficient radical scavengers that suppress the radical chain reaction (Wang et al., 2022; Wang et al., 2025), complicating the aerobic oxidation of KA oil. Herein, only a few catalytic systems have been developed for the KA-oil oxidation directly. For instance, a metal–organic framework (NiCu-MOF-74) catalyst was developed for the direct oxidation of KA oil with as high as 96.3 % yield of ε-CL (Xue et al., 2024). In this process, the Cu(I) and Ni(II) pairs significantly influenced the activation of both the methyne C-H bond of Cy-OH and α-C-C bond of Cy=O, which significantly promoted the production of ε-CL. NHPI-mediated $Ce(NH_4)_2(NO_3)_6$ catalyst was applied in the catalytic oxidation of KA oil, and achieved 46 % conversion of Cy-OH with 98 % selectivity of ε-CL (Du et al., 2019). $Ce(NH_4)_2(NO_3)_6$ in this reaction acted as a radical initiator for Cy-OH oxidation to facilitate the overall activity. However, MOF and NHPI catalysts were expensive and might leave residual Co, Cu or Ni in the lactone, deteriorating polymer properties and causing environmental concern upon degradation (Markowicz et al., 2019).

Metal-free carbon catalysts are inexpensive, environmentally benign, and possess tunable electronic structures, which are widely applied as the heterogeneous catalysts for the selective oxidation of hydrocarbons, including cyclohexane, toluene, ethylbenzene and styrene (Fu et al., 2020; Tang et al., 2016; Zhang et al., 2025). Typically, the sp^2-hybridized graphitic surface strengthens the π–π interactions between the nanocarbon and substrates, facilitating the formation, propagation, and selective transformation of radical intermediates, boosting the catalytic performance (Cai et al., 2025). In the field of ε-CL synthesis, carbon materials were found to be the superior catalysts. For instance, Ketjen black was reported as the efficient catalyst for the BV oxidation of Cy=O toward ε-CL with 91 % yield (Nabae et al., 2013). Graphite was also found to promote the reaction to produce ε-CL with a yield of 93.1 % (Li et al., 2013). Our earlier work demonstrated that N doped carbon nanotubes (NCNTs) could efficiently initiate the reaction at the low reaction temperature (~ 35 °C), affording 10.06 % yield of ε-CL (Cai et al., 2022). N doping would markedly enhance the overall activity by enhancing the interactions between nanocarbons and peroxy radicals, which derived from the aromatic or aliphatic aldehydes (Cai et al., 2022; Cai et al., 2025; Hu et al., 2025; Huang et al., 2026). Moreover, in the presence of nanocarbon, benzaldehyde (BZA), and cyclohexane as the substrates were found be oxidized to produce ε-CL (26.2 % conversion, 87.4 % selectivity) at the mild conditions (Huang et al., 2022). In this process, the KA oil as the intermediate products were produced, and the mechanism study still focused on the role of Cy=O during the free-radical reaction route. Nevertheless, the influence of Cy-OH in this process was not fully investigated.

It has been observed that BV oxidation with O_2/aldehyde exhibits strong exothermicity in both metal-catalyzed and metal-free systems (Zhang et al., 2019). To achieve high conversion of Cy=O, a large excess of aldehyde is typically required. Consequently, reactions are usually performed in dilute solution to mitigate safety risks, which, however, significantly reduces the production capacity and economic viability. Therefore, developing a solvent-free reaction system with high activity and acceptable aldehyde efficiency (AE) is a promising protocol for the production of ε-CL. In the previous study, we found that the solvent-free BV oxidation of Cy=O with O_2/aldehyde catalyzed by NCNTs could be effectively initiated, offering as high as 2964.80 mmol $g^{-1}h^{-1}$ of ε-CL, which were 2–4 orders of magnitude higher than that of traditional catalysts (Cai et al., 2022). Meanwhile, a high value of AE (~0.73) was observed in this process. These results paved a feasibility and possibility of BV oxidation catalyzed by nanocarbons under the solvent-free conditions to obtain the high production capacity and economic viability.

Inspired by the aforementioned studies, the high efficient and economic viability of solvent-free synthesis of ε-CL from KA oil using nanocarbons (i.e., CNTs and NCNTs) as the catalysts with O_2/BZA was developed in this work. The intrinsic roles of N dopants and surface oxygen functionality on lowering the apparent activation barrier, facilitating the reaction, and enhancing the AE were fully revealed. A kinetic model for the oxidation of KA oil to ε-CL catalyzed by nanocarbons was established, and the parameters such as the rate constants, activation energy and reaction orders were determined. Subsequently, the flow-sheet simulation and economic analysis demonstrate that the proposed process was both technically feasible and economically competitive for industrial implementation.

2. Result and discussion

2.1. Catalytic performance

In this work, a one-pot with high-yield route for the production of ε-CL using nanocarbon materials as the catalysts, KA oil as the substrate, molecular oxygen as the terminal oxidant and BZA as the co-oxidant was developed. KA oil specifically denotes the combined concentration of Cy-OH and Cy=O in the reaction system. Based on the previous publications, the BZA molecule was firstly activated on the nanocarbon surface and reacted with O_2 to generate the peroxybenzoic acid (Chen et al., 2025), which then participated in three parallel reaction pathways: (**SI**) reacting with Cy-OH via the dehydrogenation process yielding Cy=O (Fang et al., 2024; Moudjahed et al., 2022); (**SII**) reacting with Cy=O via a Baeyer-Villiger oxidation process to afford ε-CL (Sun et al., 2025); (**SIII**) the self-decomposition of peroxydes towards benzoic acid (BA). The overall reaction sequence starting from KA oil could be summarized in the following equations:

The physicochemical properties of various carbon catalysts and their performance in the selective oxidation of KA oil towards ε-CL are sum-

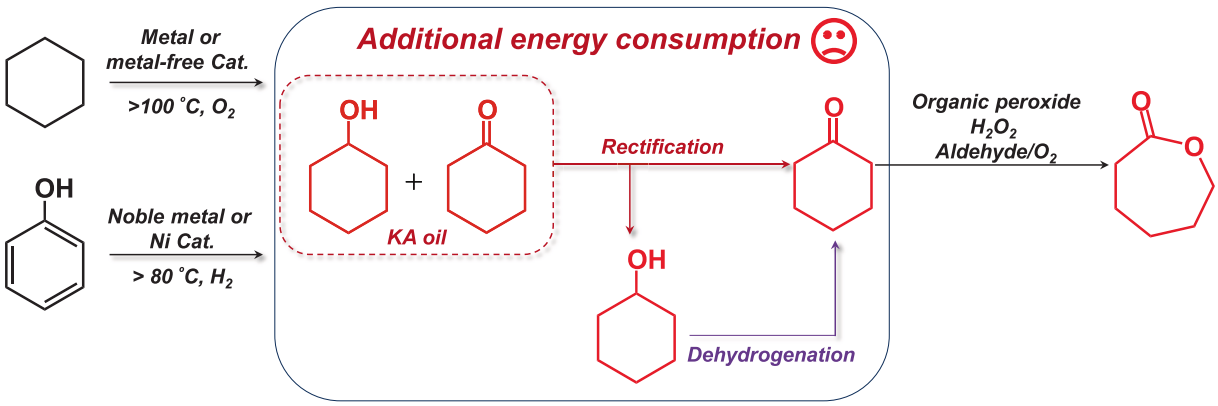

Fig. 1. The traditional route for the synthesis of ε-CL.

marized in Table 1. In the blank experiment, the conversion of KA oil was 2.39 %, while the conversions of Cy-OH and BZA were 4.38 % and 12.69 %, respectively. This comparable low conversion of KA oil could be ascribed to the self-oxidation of BZA (Cai et al., 2022; Huang et al., 2022). In this process, a ratio of K/A ($\Delta n_{Cy-OHto\varepsilon-CL}/\Delta n_{Cy=Oto\varepsilon-CL}$) was calculated to be 0.91, indicating that the transformation of Cy-OH to ε-CL was comparable to that of Cy=O to ε-CL. The addition of a typical carbon catalyst (AC) (**Fig. S1 and S2**) could mildly enhance the conversion of KA oil and BZA to 4.29 % and 19.43 %, respectively, higher than that of the blank experiment. While R_s and R_m remained as low as 0.15 mmol $m^{-2}h^{-1}$ and 185.89 mmol $g^{-1}h^{-1}$, respectively. With respect to CNTs (**Fig. S3a–b**), a remarkable enhancement of the activity was observed: the conversion of KA oil and BZA were increased to 11.87 % and 51.51 %, respectively, with the considerable R_s and R_m rising to 6.31 mmol $m^{-2}h^{-1}$ and 923.22 mmol $g^{-1}h^{-1}$. Also, the CNT system delivered an STY of 25.29 g $L^{-1}h^{-1}$ and an AE of 0.28. These results derived from the CNTs-catalyzed system were superior to those of AC, which might be resulted from the high content of surface oxygen functionalities on the surface of AC, even though a high specific surface area (SSA) of AC (1203.97 m^2 g^{-1}) was obtained (Deng et al., 2020; Huang et al., 2026). When NCNTs (with 3.35 at.% N, **Fig. S3c-d**) was used as the catalysts, a further improved catalytic performance was observed. In this reaction, the conversion of KA oil and BZA increased to 19.68 % and 69.79 %, respectively, with the high normalized activities (10.79 mmol $m^{-2}h^{-1}$ and 1530.67 mmol $g^{-1}h^{-1}$), while the selectivity of ε-CL reached 93.27 % and the value of AE increased to 0.37, demonstrating that N doping was the highly effective protocol for improving the oxidation of KA oil. The STY and E-factor were 41.93 g $L^{-1}h^{-1}$ and 2.76, respectively, indicating good potential for industrial application. Notably, the conversion of Cy-OH was 39.12 % and the ratio of K/A was 2.00, much higher than that of AC (1.01) and CNTs (1.54), indicating that the N doping could greatly improve the transformation of Cy-OH to ε-CL. We believe that NCNTs promoted the initial alcohol oxidation step more effectively, leading to a higher accumulation of Cy=O in the reaction system, which would facilitate the subsequent production of ε-CL, resulting in a higher overall activity. Meanwhile, the enhanced K/A ratio provided indirect evidence that NCNTs facilitate the first oxidation step in the consecutive reaction pathway. This activity catalyzed by NCNTs showed the superior catalytic performance over the traditional catalyst NHPI/CAN system (Chen et al., 2025), in which the 73.60 % conversion of KA oil and 34.00 % Cy-OH conversion with 98.00 % ε-CL selectivity were obtained.

The selective oxidation of hydrocarbon in the liquid-phase catalyzed by nanocarbons generally underwent a radical-chain process, as confirmed in the previous publications for the generation of ε-CL from the Cy=O oxidation (Ma et al., 2021; Zhai et al., 2025). In this work, 3 mmol of p-benzoquinone as the radical scavenger was added into the reaction, and the reaction was significantly suppressed (0.12 % conversion of KA oil), confirming that this oxidation of KA oil with the presence of BZA/O_2 was proceeded via a free-radical mechanism. The electron paramagnetic resonance (EPR) measurements further revealed that the formation of superoxide radicals during the reaction (**Fig. S4**). When NCNTs were used, a much stronger superoxide signal was detected, whereas no apparent signal was observed in the blank, in line with the observed catalytic activities. These results indicated that NCNTs markedly promoted superoxide-radical generation and thereby accelerated the reaction (Shi et al., 2022; Tiwari et al., 2018). Moreover, to verify the role of different substrates during the oxidation of KA oil towards ε-CL, substrate-scope experiments were subsequently carried out. When BZA was omitted, KA oil conversion fell to 0.32 %, demonstrating that BZA acted as an indispensable co-oxidant. 15.43 % conversion of Cy=O with an AE of 0.54 was obtained when Cy-OH was absent, following a typical Baeyer–Villiger oxidation process(Cai et al., 2022). When Cy=O was excluded and only Cy-OH and BZA were present, the system was almost inactive (Cy-OH conversion 0.04 %, no ε-CL), showing that Cy-OH could not be directly oxidized to ε-CL without Cy=O, which functioned as an initiator in this process. Furthermore, a high stability of NCNTs in this reaction was observed after five recycle runs (**Fig. S5**). The relative characterization (including TEM and Raman) results demonstrated that there was no apparent change of NCNTs was obtained during the reaction.

The time-dependent activities of the NCNT- and CNT-catalyzed systems were compared (Fig. 2**a-b** and **Table S1**). When CNTs was used as the catalyst, the decrease concentration of Cy-OH decreased gradually from 1.77 to 1.28 mol L^{-1} within 5 h. Accordingly, the concentration of ε-CL increased from 0 to 0.75 mol L^{-1}. The significant change of the concentrations of Cy-OH (from 1.74 to 0.87 mol L^{-1}) and ε-CL (from 0 to 0.95 mol L^{-1}) were observed when NCNTs was applied, especially the sharply variations of BZA within 1 h. Notably, the concentration profiles of Cy=O were almost identical in the two systems, due to the

Table 1
Catalytic performance of various catalyst for the KA oil oxidation for the production of ε-CL.[a].

Entry	Catalyst	S_{BET} [b] (m^2 g^{-1})	I_D/I_G [c]	R_s [d] (mmol m^{-2} h^{-1})	R_m [e] (mmol g^{-1} h^{-1})	Conversion (%) KA oil	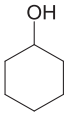	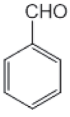	Selectivity (%) 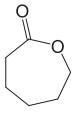	K/A [f]	STY [g] (g L^{-1} h^{-1})	AE [h]	E-factor [i]
1	Blank	–	–	–	–	2.39	4.38	12.69	95.84	0.91	5.09	0.26	1.19
2	AC	1203.97	0.79	0.15	185.89	4.29	5.54	19.43	96.73	1.01	9.14	0.25	3.36
3	CNTs	146.16	0.64	6.31	923.22	11.87	33.18	51.51	91.03	1.54	25.29	0.28	3.46
4	NCNTs [j]	141.87	0.92	10.79	1530.67	19.68	39.12	69.79	93.27	2.00	41.93	0.37	2.76
5	NCNTs [k]	141.87	0.92	–	–	0.12	0.12	0.78	99.99	–	0.25	–	–
6	NCNTs [l]	141.87	0.92	8.45	1200.11	15.43	–	61.54	94.74	–	32.88	0.54	3.12
7	NCNTs [m]	141.87	0.92	–	–	0.32	0.32	–	99.99	–	0.68	–	–
8	NCNTs [n]	141.87	0.92	–	–	0.04	0.04	0.45	–	–	0.09	–	–
9	NHPI/CAN [o]	–	–	–	–	73.60	34.00	–	98.00	–	–	–	–

[a] Conditions: 45 °C, 12 mg catalyst, 3 h, 1100 rpm, 60 mL/min O_2, 0.19 mol Cy=O, 0.09 mol Cy-OH, 0.19 mol BZA. [b] Data from N_2 adsorption–desorption isotherm of different catalysts (**Fig. S1**). [c] Data from Raman spectral results (**Fig. S2**). [d] Initial rate of KA oil consumption per m^2 of catalyst surface area with a low-conversion of KA oil (<10 %). [e] Initial rate of KA oil consumption per gram of catalyst with a low-conversion of KA oil (<10 %). [f] The ratio of $\Delta n_{Cy-OHto\varepsilon-CL}/\Delta n_{Cy=Oto\varepsilon-CL}$. [g] STY = $m_{product}/(V_{reactor} \times t)$. [h] AE, calculated by (produced molar amount of ε-CL)/(consumed molar amount of BZA). [i] E-factor = $m_{waste}/m_{product}$. [j] NCNTs are represented as NCNTs-3.35. [k] With 3 mmol p-benzoquinone. [l] Without Cy-OH. [m] Without BZA. [n] Without Cy=O. [o] 10 mmol Cy-OH, 15 mmol Cy=O, 30 g 1,1,1,3,3,3-hexafluoro-2 propanol(HFIP), 1 atm, 600 rpm, 45 °C, 37 h, Ref. (Du et al., 2019).

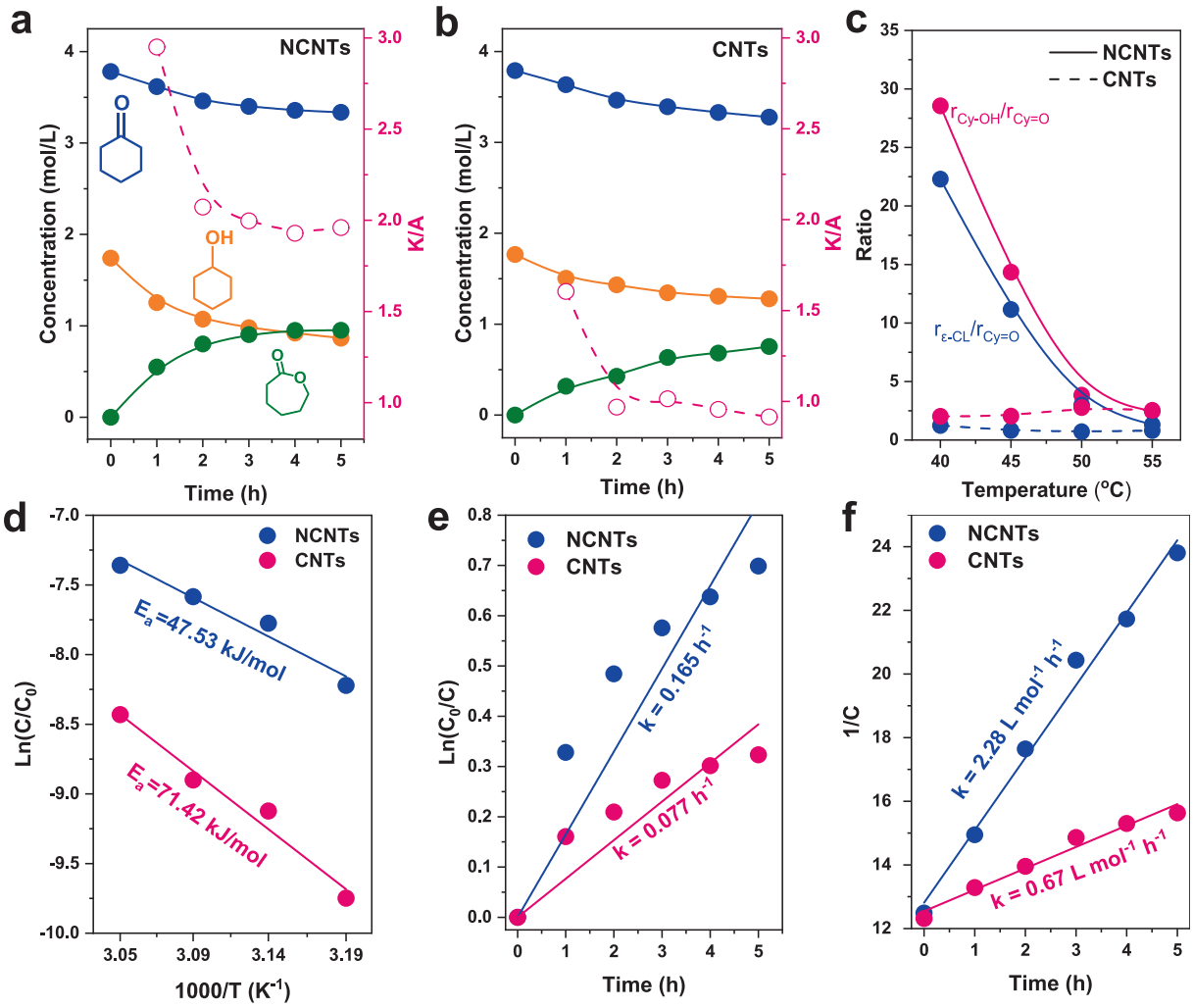

Fig. 2. The plotting of reaction time vs. the molarity of substrates/products catalyzed by NCNTs (a) and CNTs (b). Conditions: 45 °C, 12 mg catalyst, 3 h, 0.19 mol Cy=O, 0.19 mol BZA, 0.09 mol Cy-OH, 60 mL/min O_2 (c). Dependence of ratios on the temperature over NCNTs and CNTs. (d) Arrhenius plots of Cy-OH oxidation catalyzed by NCNTs and CNTs. (e) Pseudo-one order and (f) pseudo-second order reaction plotting of Cy-OH oxidation catalyzed by NCNTs and CNTs.

intermediate role of Cy=O bridging the Cy-OH oxidation and the BV oxidation yielding the ε-CL (**Eqs. 1–3**). In contrast, the concentrations of Cy-OH and ε-CL varied significantly, confirming that Cy-OH was the main precursor of the lactone.

Based on the aforementioned discussions, we can conclude that the conversion of Cy-OH to Cy=O was the initial step (**SI**) for the reaction, and the BV oxidation of Cy=O towards ε-CL (**SII**) was the second step. The verification of the reaction rate for each step would benefit in understanding the difference of these activities over NCNTs and CNTs, which were noted as the consumption rates of Cy-OH (r_{Cy-OH}), Cy=O ($r_{Cy=O}$), and the generation rate of ε-CL ($r_{\varepsilon-CL}$). Especially, the parameters of $r_{Cy-OH}/r_{Cy=O}$ and $r_{\varepsilon-CL}/r_{Cy=O}$ revealed the extent of reaction between two steps (Fig. 2**c**). Over NCNTs, the value of the $r_{Cy-OH}/r_{Cy=O}$ (from 28.56 to 2.45) was decreased along with the increase of the reaction temperature (40 °C to 55 °C), demonstrating that the transformation of Cy-OH towards Cy=O was greatly enhanced by NCNTs at low reaction temperature. And the high temperature would comparably enhance the consumption of Cy=O, thus lowering the value of $r_{Cy-OH}/r_{Cy=O}$. Meanwhile, the similar tendency of the value of $r_{\varepsilon-CL}/r_{Cy=O}$ (from 22.29 to 1.31) was observed. These results demonstrated that under the comparable low reaction temperature (< 50 °C), r_{Cy-OH} was close to $r_{\varepsilon-CL}$, while a low $r_{Cy=O}$ was present. When the temperature was higher than 50 °C, $r_{Cy=O}$ was facilitated to balance the reaction rate of SI and SII, thus more Cy-OH could be oxidized to produce ε-CL. Notably, when CNTs as the catalyst was used, the low values of $r_{Cy-OH}/r_{Cy=O}$ and $r_{\varepsilon-CL}/r_{Cy=O}$ with insensitivity to temperature were observed, indicating that the CNTs could not significantly tune the reaction route and facilitate the reaction.

On the basis of the aforementioned discussions, we believed that the oxidation of Cy-OH was the key step for the reaction, which could be chosen as the reference step for activation-energy and pseudo-second-order kinetic analyses. As shown in Fig. 2**d**, the Arrhenius plots over CNTs- and NCNTs-catalyzed systems were conducted (**Table S2**). The apparent activation energies for NCNTs and CNTs were calculated to be 47.5 and 71.4 kJ mol^{-1}, respectively, revealing that N doping substantially lowered the energy barrier in this carbon-catalyzed process. A rational pseudo-second-order fitting, instead of pseudo-one-order fitting (Fig. 2**e** and Fig. 2**f**), was obtained, offering the rate constants of 2.28 L mol^{-1}h^{-1} for NCNTs and 0.67L mol^{-1}h^{-1} for CNTs. The superior fit of the pseudo-second-order kinetic model, as opposed to the pseudo-first-order model, indicated that the overall reaction rate was governed by coupled transformations rather than a single-reactant-controlled step. Mechanistically, this aligned with the consecutive nature of the process: Cy-OH was initially converted to Cy=O, which subsequently served as the critical intermediate for ε- CL synthesis. Consequently, the kinetic dependence on the concentrations of both species strongly corroborated a reaction network dominated by consecutive, surface-mediated transformations. These results further confirmed the superior ability of

NCNTs to promote the transformation of Cy-OH to ε-CL.

Previous studies have shown that N doping on the surface of nanocarbon materials could significantly enhance catalytic activity (Cao et al., 2014; Fu et al., 2020; Yu et al., 2011), which was considered as the crucial active site. Based on the literature and our earlier publications, the BV oxidation reaction in an aldehyde/oxygen system could be efficiently facilitated with the presence of carbon catalysts, and we observed a volcano-shaped trend between the surface N content of carbons and their catalytic activity (Cai et al., 2022; Huang et al., 2026). In this study, a series of NCNTs with varying N contents (1.12–4.82 at.%) by controlling the pyrolysis deposition time were prepared (Table 2). The SSA of NCNTs slightly decreased with increasing N content, probably due to coverage of the mesoporous surface by deposited carbon layers. The I_D/I_G ratios of these NCNTs ranged from 0.73 to 0.92, and the surface defect density initially increased and then decreased with N content, reaching a maximum for NCNTs-3.35 (I_D/I_G = 0.92). As N contents was below 3.35 at.%, the defects mainly originated from edge carbon and N species in the deposited carbon layers. In contrast, at higher N contents, excessive carbon deposition covered some edge sites and blocked pores, thereby reducing the overall defect density. Notably, all NCNTs exhibited higher defect densities than pristine CNTs, confirming that N doping effectively enhanced the surface defect density (**Fig. S2**).

The catalytic performance over various carbon catalysts were evaluated. Compared to CNTs, even a low content of N dopant (1.12 at. %), a considerable improvement in reaction performance was observed (19.11 % conversion of KA oil). After that, a fluctuating activity within the range of 19.68–21.92 % (KA oil) was observed. In this process, the oxidation of Cy-OH firstly increased and then decreased accordingly with the highest conversion of Cy-OH (39.12 %) over NCNTs with 3.35 at. % N dopant. Meanwhile, the introduction of N dopants would significant modulate the surface-area-normalized reaction rate (R_s) and mass-specific reaction rate (R_m) (Fig. 3**a**), in which the value of R_s varied between 8.91 and 12.41 mmol m^{-2} h^{-1}, and that of R_m ranged from 1408.56 to 1704.89 mmol g^{-1} h^{-1}, substantially higher than the corresponding values for CNTs (6.31 mmol $m^{-2}h^{-1}$ and 923.22 mmol $g^{-1}h^{-1}$). Simultaneously, the space–time yield increased from 25.29 g $L^{-1}h^{-1}$ to 40.02 g $L^{-1}h^{-1}$ (Fig. 3**b**). These results confirmed that N doping could efficiently facilitate the production of ε-CL from the KA oil. Notably, the values of AE (~ 0.37) and E-factor (~ 2.76) over NCNT-catalyzed system were not influenced by the N dopant (Fig. 3**c**), which, nevertheless, were much better than those of CNT-catalyzed system (0.28 for AE and 3.46 for E-factor, respectively), further demonstrating that N doping could contribute to a high efficiency and environmentally benign process. Also, the value of K/A first increased and then decreased with a maximum value of K/A over NCNTs-3.35 (2.00). Additionally, KA oil conversion stabilized in the range of 19.11–21.92 % in the NCNT-catalyzed system, higher than that in the CNT-catalyzed system (11.87 %), suggesting that NCNTs preferentially catalyze the oxidation of Cy=O over that of Cy-OH.

In catalytic processes, N species on carbon surfaces are considered to play crucial roles, where N configurations have been reported to effectively modulate activity in various reactions, including electrochemical reactions, selective oxidation, hydrochlorination, and dehydrogenation (Chen et al., 2010; Chizari et al., 2010; Gong et al., 2009; Ning et al., 2019). For instance, the N configurations (especially N_P and N_G) in carbon materials with varied content ratios and distances between those N species would significantly influence the catalytic performance of NCNTs in the selective epoxidation of styrene (Fu et al., 2020). Our previous work demonstrated that the ratio of graphitic N (N_G) to pyridinic N (N_P) strongly influenced the activity of nanocarbons in the BV oxidation of Cy=O in the liquid-phase(Cai et al., 2022; Huang et al., 2022), underscoring the significance of N species and distribution (Huang et al., 2026). Here, the major N species were identified on the carbon surface by XPS analysis, including N_P (398.3 ± 0.1 eV), pyrrolic N (N_{Pyr}, 399.5 ± 0.1 eV), N_G (401 ± 0.1 eV), nitrogen oxides (N_{OX}, 403

Table 2
The catalytic oxidation of KA oil over NCNTs with different content of N dopants. [a].

Catalyst	Gross N [b] (at.%)	N species [c] (at.%)			N_G/N_P	S_{BET} [d] (m^2 g^{-1})	I_D/I_G [e]	Rs [f] (mmol m^{-2} h^{-1})	Rm [g] (mmol g^{-1} h^{-1})	Conversion (%) KA oil	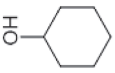	Selectivity (%) 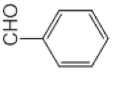	K/A [h]	STY [i] (g L^{-1} h^{-1})	AE [j]	E-factor [k]
	–	N_P	N_{Pyr}	N_G												
CNTs	–	–	–	–	–	146.16	0.64	6.31	923.22	11.87	33.18	51.51	91.03	1.01	25.29	0.28	3.46
NCNTs-1.12	1.12	0.32	0.17	0.27	0.84	158.12	0.81	8.91	1408.56	19.11	29.52	59.69	82.09	1.76	33.42	0.37	2.76
NCNTs-2.18	2.18	0.26	0.20	0.34	1.30	144.08	0.82	11.83	1704.89	21.92	36.46	68.59	81.32	1.87	37.98	0.37	2.79
NCNTs-3.35	3.35	0.25	0.20	0.38	1.52	141.87	0.92	10.78	1529.35	19.68	39.12	69.79	93.27	2.00	39.11	0.37	2.76
NCNTs-4.82	4.82	0.25	0.17	0.42	1.68	130.52	0.73	12.41	1620.11	20.83	33.02	63.16	90.13	1.67	40.02	0.38	2.71

[a] Conditions: 45 °C, 12 mg catalyst, 3 h, 1100 rpm, 60 mL/min O_2, 0.19 mol BZA, 0.09 mol Cy=O, 0.19 mol Cy-OH. [b] XPS data was obtained from **Fig. S6** [c] High-resolution N_{1s} XPS spectra of NCNTs catalysts were obtained from Fig. 2**a**. N_P, N_{Pyr}, and N_G respectively represent pyridine nitrogen, pyrrole nitrogen, and graphite nitrogen. [d] The SSA of NCNTs were obtained from **Fig. S7**. [e] The surface defect of NCNTs were obtained from **Fig. S8**. [f] Initial rate of KA oil consumption per m^2 of catalyst surface area with a low-conversion of KA oil (<10 %). [g] Initial rate of KA oil consumption per gram of catalyst with a low-conversion of KA oil (<10 %). [h] The ratio of $\Delta n_{Cy-OHtoε-CL}/\Delta n_{Cy=OtoE-CL}$. [i] STY = $m_{product}/(V_{reactor} \times t)$. [j] AE, calculated by (produced molar amount of ε-CL)/(consumed molar amount of BZA). [k] E-factor = $m_{waste}/m_{product}$.

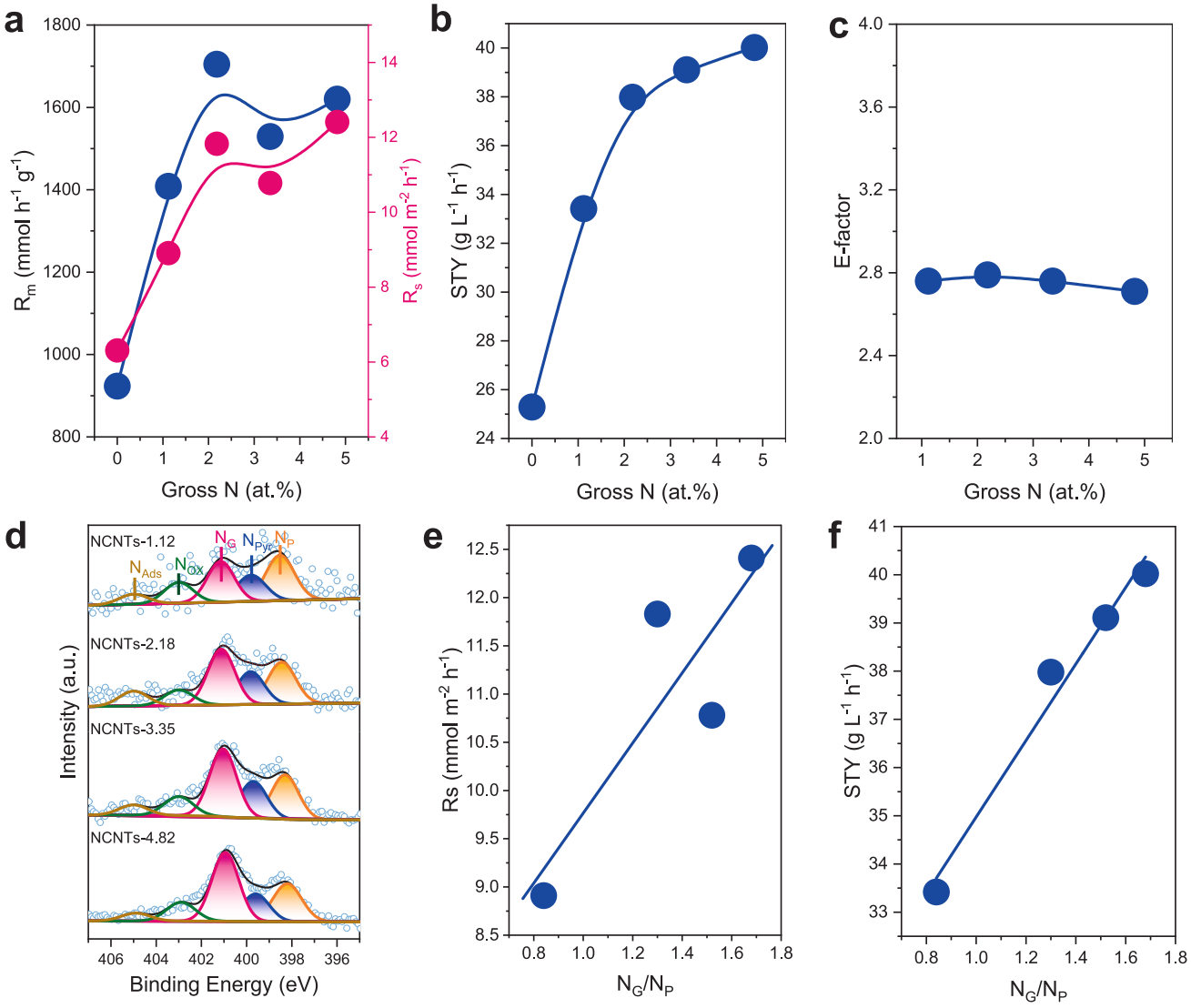

Fig. 3. (a) Dependence of the consumption rate on the gross N. Dependence of STY (b) and E-factor (c) on the gross N content. (d) High-resolution deconvolution of N *1 s* XPS spectra of NCNTs catalysts. Dependence of R_s (e) and STY (f) on the ratio of N_G/N_P.

± 0.2 eV), and chemisorbed N species (N_{co}, 404.9 ± 0.1 eV) (Fig. 3**d**) (Cao et al., 2017; Wei et al., 2015). The plotting between N species (mainly N_P, N_{Pyr}, and N_G) and reaction activity demonstrated that there were chaotic relationships between the individual N species and R_m or R_s (**Fig. S9 and S10**). Nevertheless, the positive relationships between the ratio of N_G/N_P and R_s were obtained (Fig. 3**e**), indicating that the KA oil oxidation was also greatly influenced by the N configuration and their contents. Similarly, N species such as N_P and N_G showed the opposite relationships with STY (**Fig. S11**), indicating that N_G would promote the ε-CL formation, whereas N_P did not. Therefore, a positive relationship between N_G/N_P and STY could be observed (Fig. 3**f**), agreeing with our earlier findings that the N_G/N_P ratio played a critical role in the BV oxidation (Huang et al., 2026). These results demonstrated that increasing the N_G/N_P ratio would significantly enhance both the reaction rate and ε-CL productivity, establishing the N_G/N_P ratio as a key descriptor for tuning the catalytic performance of NCNTs in the synthesis of ε-CL from KA oil.

To elucidate how nitrogen configurations affect catalytic performance, the density functional theory (DFT) calculations were performed to investigate the adsorption energies between the model carbons (graphene (G), G with N_G (N_G), G with N_G and N_P (N_G/N_P), and G with 2 N_G atom and N_P ($(2N_G)/N_P$)) and different substrates (Cy-OH, Cy=O, and BZA) (Fig. 4 and **Table S3**). The adsorption energies of Cy-OH on these four N configurations were −0.12, −0.43, −0.46, and −0.48 eV, respectively. This indicated that N-doping enhanced Cy-OH activation, an effect further promoted by increasing N_G content. BZA adsorption followed a similar trend, strengthening from −0.09 eV on G to −0.12, −0.17, and −0.25 eV on N_G, N_G/N_P, and $(2N_G)/N_P$, suggesting that N_G also facilitated BZA interaction. Conversely, Cy=O adsorption was highly sensitive to the N configuration, with energies of −1.04, −0.32, −1.27, and −0.67 eV on G, N_G, N_G/N_P, and $(2N_G)/N_P$, respectively. It was notable that N_P site was the key active site for enhancing the adsorption of Cy=O on the carbon surface, while N_G was not, which was different from other substrates. Our previous work demonstrated that N_G sites would be more favorable for adsorbing BZA instead of Cy=O, lowering the overall activity (Cai et al., 2025). Meanwhile, the presence of N_P sites would improve the interaction between Cy=O and carbon catalyst. In this work, Cy=O was a crucial intermediate for ε-CL generation, the key step for the overall activity, meaning that the catalytic activity increased alone with content of N_P sites. These results were consistent with the data in Fig. 3**d and e**. Therefore, a higher N_G/N_P ratio does not merely enhance all adsorption, rather, it establishes a vital adsorption balance. It boosts the surface enrichment of Cy-OH and BZA while preventing the over-binding of Cy=O, thereby driving the

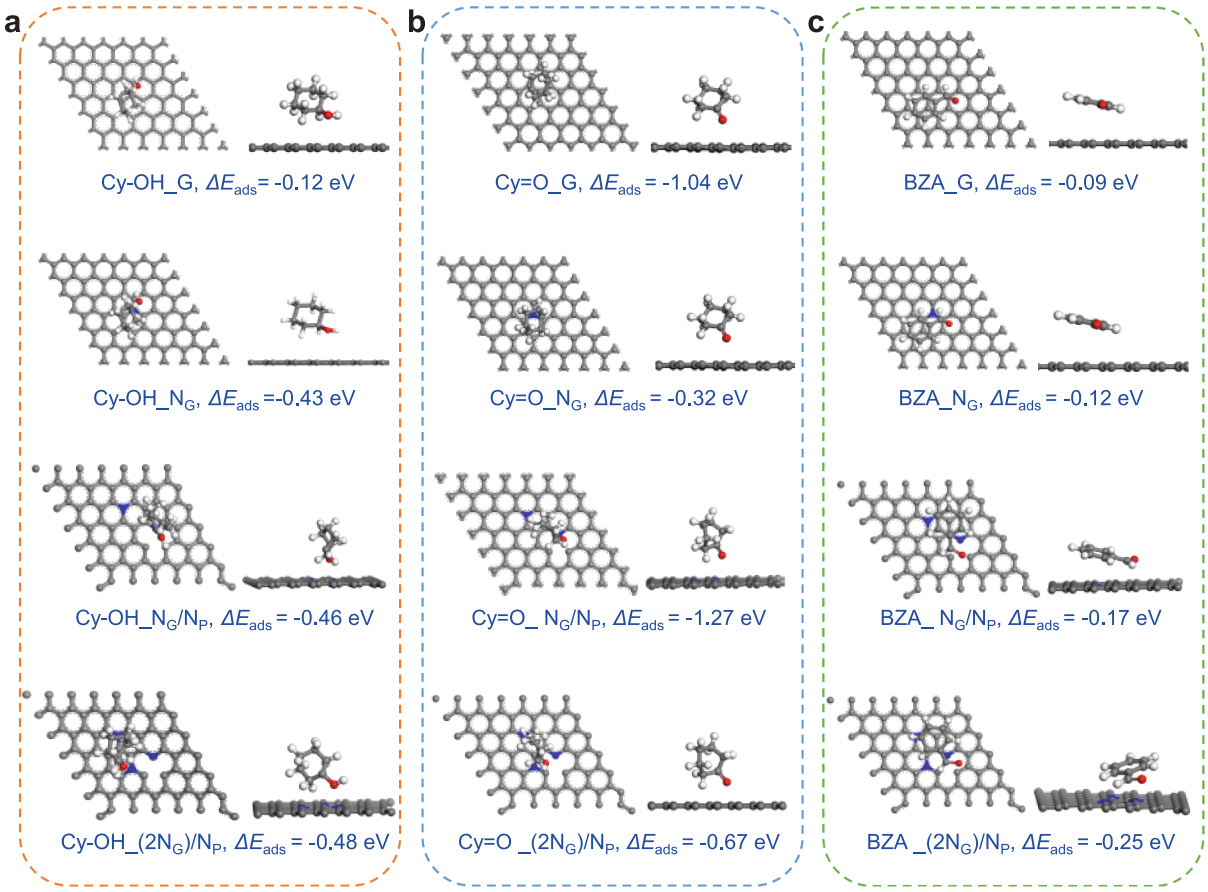

Fig. 4. Stable configurations and adsorption energy of substrates-carbon complexes from the DFT calculations.

continuous Cy-OH → Cy=O → ε-CL cascade.

Surface oxygen functionalities were known to suppress the propagation of the free-radical in the liquid-phase reactions catalyzed by nanocarbons(Chi et al., 2016; Kim et al., 2019), yet their presence had been reported to improve AE in BV oxidations(Cai et al., 2022). In this study, the influence of the surface oxygen functionalities of NCNTs on the selective oxidation of KA oil was detailed (Table 3). Various carbon catalysts with different O content underwent the HNO_3 treatment and high-temperature annealing processes. Four kinds of carbon catalysts including the pristine NCNTs-3.35, NCNTs-3.35 annealed at 1000 °C (NCNTs-1000), NCNTs-1000 under the HNO_3 treatment (NCNTs-1000–7), and NCNTs-1000–7 annealed at 800 °C (NCNTs-1000–7-800). Since the oxygen functionalities would be removed underwent the annealing process, while would be introduced via the HNO_3 treatment, the oxygen contents over these four kinds of catalysts were 1.41 at.%, 1.09 at.%, 2.69 at.%, and 1.05 at.%, respectively. Meanwhile, these treatments would produce more mesoporous carbons or surface defects on the carbon catalysts, thus improving the SSA of these catalysts.

Subsequently, these carbon materials with different O content were used in the KA oil oxidation. NCNTs-1000 afforded 20.04 % conversion

Table 3
The catalytic oxidation of KA oil over NCNTs with different content of oxygen-containing groups. [a].

Entry	Catalyst	O [b] (at. %)	S_{BET} [c] (m^2 g^{-1})	R_s [d] (mmol m^{-2} h^{-1})	R_m [e] (mmol g^{-1} h^{-1})	Conversion (%) KA oil	OH	CHO	Selectivity (%) O	K/A [f]	STY [g] (g L^{-1} h^{-1})	AE [h]	E-factor [i]
1	Blank	–	–	–	–	2.39	4.38	12.69	95.84	0.91	–	0.26	–
2	NCNTs[j]	1.41	141.87	10.78	1529.35	19.68	39.12	69.79	93.28	2.00	41.93	0.37	1.55
3	NCNTs-1000	1.09	183.56	8.49	1558.67	20.04	38.54	69.29	81.84	1.98	42.70	0.34	1.71
4	NCNTs-1000–7	2.69	207.01	4.46	923.26	8.85	12.24	27.84	87.10	1.03	18.86	0.39	2.62
5	NCNTs-1000–7-800	1.05	238.71	6.41	1530.13	17.86	33.95	66.14	81.42	1.78	38.05	0.31	3.30

[a] Conditions: 45 °C, 12 mg catalyst, 3 h, 1100 rpm, 60 mL min^{-1} O_2, 0.19 mol Cy=O, 0.19 mol BZA, 0.09 mol Cy-OH. [b] XPS data was obtained from **Fig. S12**. [c] The SSA of NCNTs were obtained from **Fig. S13.** [d] Initial rate of KA oil consumption per m^2 of catalyst surface area with a low-conversion of KA oil (<10 %). [e] Initial rate of KA oil consumption per gram of catalyst with a low-conversion of KA oil (<10 %). [f] The ratio of $\Delta n_{Cy-OHto\varepsilon-CL}/\Delta n_{Cy=Oto\varepsilon-CL}$. [g] STY = $m_{product}/(V_{reactor} \times t)$. [h] AE, calculated by (produced molar amount of ε-CL)/(consumed molar amount of BZA). [i] E-factor = $m_{waste}/m_{product}$. [j] NCNTs-3.35.

of KA oil and 38.54 % of Cy-OH, with R_s and R_m were 8.49 mmol $m^{-2}h^{-1}$ and 1558.67 mmol $g^{-1}h^{-1}$, respectively, which were close to that of the pristine NCNTs. In contrast, the HNO_3-treated sample (NCNTs-1000–7) exhibited a pronounced decrease in activity. The conversion of KA oil and Cy-OH fell to 8.85 % and 12.24 %, respectively. And R_s and R_m decreased to 4.46 mmol $m^{-2}h^{-1}$ and 923.26 mmol $g^{-1}h^{-1}$, respectively. This result demonstrated that the introduction of surface oxygen functionality still suppressed the activity. NCNTs-1000–7-800 with a lowered O content (1.05 at. %) apparently restored the catalytic performance (17.86 % KA oil conversion, 6.41 mmol $m^{-2}h^{-1}$, and 1530.13 mmol $g^{-1}h^{-1}$), indicating that the surface oxygen functionalities were not the active sites for the reaction. The change of K/A ratio over these catalysts demonstrated that the introduction of oxygen functionalities would not benefit the process of Cy-OH to ε-CL, in which a value of 1.03 for NCNTs-1000–7 was observed. In contrast, 1.98 and 1.78 were observed for NCNTs-1000 and NCNTs-1000–7-800, respectively. It was noted that the value of AE slightly enhanced after the introduction of oxygen functionalities. For instance, 0.37 and 0.39 of AE over NCNTs and NCNTs-1000–7, respectively, were observed, which were higher than that of NCNTs-1000 (0.34) and NCNTs-1000–7-800 (0.31). This phenomenon was consistent with our previous observations (Cai et al., 2022; Chi et al., 2016). Moreover, E-factor for these catalysts ranked as following: NCNTs (1.55) < NCNTs-1000 (1.71) < NCNTs-1000–7 (2.62) < NCNTs-1000–7-800 (3.30), implying that both treatment would deteriorate the capability of catalysts in this reaction with a view of atomic economy. Interestingly, it was observed that a decrease in oxygen content on carbon surface resulted in enhanced catalytic activity (8.85 % for NCNTs-1000–7, 17.86 % for NCNTs-1000–7-800), but decreased the ε-CL selectivity (87.10 % for NCNTs-1000–7, 81.42 % for NCNTs-1000–7-800). The earlier publications of our group demonstrated that the presence of oxygen functionalities would greatly affect the catalytic activity of carbon catalysts in the selective oxidation, including cyclohexane oxidation, cumene oxidation, ethylbenzene oxidation etc (Cao et al., 2014; Chi et al., 2016; Yu et al., 2011). For the BV oxidation of Cy=O, we observed the similar tendency in the previous work, in which the activity was suppressed even at very low oxygen contents, while the AE was significantly enhanced with higher oxygen content (Cai et al., 2022). In other words, the oxygen functionality on carbon surface would hinder the activity, but benefit the selectivity of ε-CL by suppressing of side reactions. Here, the key step from Cy=O to ε-CL still followed the same reaction mechanism.

2.2. Kinetic modeling

A detailed kinetic investigation was conducted to uncover the intrinsic kinetic parameters and to provide a solid theoretical basis for the potential scale-up of ε-CL production. According to the literatures and aforementioned discussions, three main reactions could be under the consideration: (i) oxidation of Cy-OH to Cy=O, (ii) BV oxidation of Cy=O to ε-CL, and (iii) undesired auto-oxidation of BZA (**Eqs. 1–3**). Based on the principle of the mass balances, reaction rates for Cy-OH (A), Cy=O (B), BZA (C), ε-CL (D), and BA (E) were efficiently set. Since oxygen was always in large excess cross the whole reaction, the change of oxygen concentration could be omitted in the rate expressions. These corresponding rate equations are listed (**Eqs. (4)–(8)**:

$$r_A = -k_1 \bullet {C_A}^l \bullet {C_C}^m \tag{4}$$

$$r_B = -k_1 \bullet {C_A}^l \bullet {C_C}^m - k_2 \bullet {C_C}^p \bullet {C_B}^q \tag{5}$$

$$r_C = -k_1 \bullet {C_A}^l \bullet {C_C}^m - k_3 \bullet {C_C}^n - k_2 \bullet {C_C}^p \bullet {C_B}^q \tag{6}$$

$$r_D = -k_2 \bullet {C_C}^p \bullet {C_B}^q \tag{7}$$

$$r_E = k_1 \bullet {C_A}^l \bullet {C_C}^m + k_3 \bullet {C_C}^n + k_2 \bullet {C_C}^p \bullet {C_B}^q \tag{8}$$

Where k_1, k_2 and k_3 were represented as the reaction rate constants for the three main elementary steps. L and m represented the reaction orders of Cy-OH and BZA in the **SI** reaction, respectively. P and q represented the reaction orders of BZA and Cy=O in the **SII** reaction, respectively. n represented the reaction orders of BZA in the **SIII** reaction. A, B, and C were represented as Cy-OH, Cy=O, and BZA, respectively.

Before the kinetic study, the effects of stirring speed and oxygen flow rate on reaction activity were systematically optimized to eliminate mass transfer limitations (**Fig. S14**). A serial sets of experiments with different substrate ratios under different reaction temperature were performed in the presence of CNTs or NCNTs as a catalyst (Fig. 5, **Table S4 and S5**). To minimize the effect of side reactions caused by excessive oxidation of BZA to BA, the extent of reaction of BZA oxidation was strictly controlled across all the experiments. The experimental data were incorporated into the established kinetic model equations (**Eqs. (4)–(8)** and numerically solved in MATLAB software using the ODE_45 model with the Runge–Kutta method (Mu et al., 2018). The fmincon function was subsequently applied to obtain the reaction rate constants (k_1, k_2, and k_3), as well as the reaction orders (l, m, n, p, and q). The regressed data and the experimental data were presented and summarized (Table 4). The results demonstrated that the simulated data agreed well with the experimental data, validating the reliability of the proposed kinetic model for the NCNTs-catalyzed system. Within the NCNTs-catalyzed system, a comparison of the rate constants ($k_{45,\ NCNTs}$) for the three main elementary steps (**SI**: the oxidation of Cy-OH to Cy=O; **SII**: the oxidation of Cy=O to ε-CL; **SIII**: the autoxidation of BZA) reveals distinct kinetic behavior. The k_{45} for three main steps was calculated to be 0.05 mol^{-1} L h^{-1}, 0.0024 $mol^{-4.42}$ $L^{-6.42}$ h^{-1}, and 0.02 $mol^{-1.69}$ $L^{-3.69}$ h^{-1}, respectively. This indicated that the oxidation of Cy-OH is the fastest step, whereas the BV oxidation of Cy=O towards ε-CL is the slowest. In other words, Cy-OH could be rapidly oxidized to Cy=O in the presence of BZA catalyzed by NCNTs, yet the subsequent reaction between Cy=O and BZA was significantly hindered when Cy-OH remained in the system, due to the radical scavenging effect of Cy-OH in this system. When CNTs was used as the catalyst, $k_{45,\ CNTs}$ with lower value across these three steps were observed (0.0332 $mol^{-0.44}$ $L^{-1.44}$ h^{-1}, 0.0011 $mol^{-2.18}$ $L^{-4.18}$ h^{-1}), and 0.0143 $mol^{-0.89}$ $L^{-2.89}$ h^{-1} for **SI, SII, and SIII**, respectively). It was noted that the similar tendency of these three reactions catalyzed by CNTs were observed, and N doping indeed could accelerate all the reaction.

The order of reaction reveals the influence of substrate concentration on the reaction activity (Deng et al., 2022; Su et al., 2023). In this study, the orders of reaction for those three steps catalyzed by CNTs and NCNTs were summarized (Table 4). As can be seen that the orders of reaction over NCNTs-catalyzed system were apparently higher than that over CNTs-catalyzed system, further conforming that N doping would effectively facilitate each reaction in the carbon-catalyzed reaction. Take **SI** as a sample, the orders of reaction over NCNTs-catalyzed system were 1.00 (Cy-OH) and 1.00 (BZA), which were higher than that over CNTs-catalyzed system (0.68 for Cy-OH and 0.76 for BZA). It was worth mentioning that the order of reaction of BZA in these three steps were higher that of the substrates for each step, showing the importance of BZA oxidation in this reaction. In **SII** with the presence of NCNCTs, the reaction orders for Cy=O and BZA were 1.74 and 3.38, respectively, higher than those in **SI,** suggesting that the presence of Cy=O accelerated the oxidation of BZA, which might also be attributed to stronger adsorption and difficult desorption of Cy=O on the carbon surface, as supported by our DFT calculations. In summary, NCNTs significantly enhance the overall reaction rates, with the most pronounced effect observed in the ε-CL formation.

Based on the rate constants obtained at different temperatures, the activation energies for each primary step were calculated (Table 4). For the three consecutive reactions, the activation energies over NCNTs were determined to be 59.11 kJ mol^{-1}, 63.14 kJ mol^{-1}, and 33.35 kJ mol^{-1}, respectively, which are all lower than those measured for CNTs (68.15 kJ·mol^{-1}, 86.88 kJ mol^{-1}, and 51.68 kJ mol^{-1}). This result

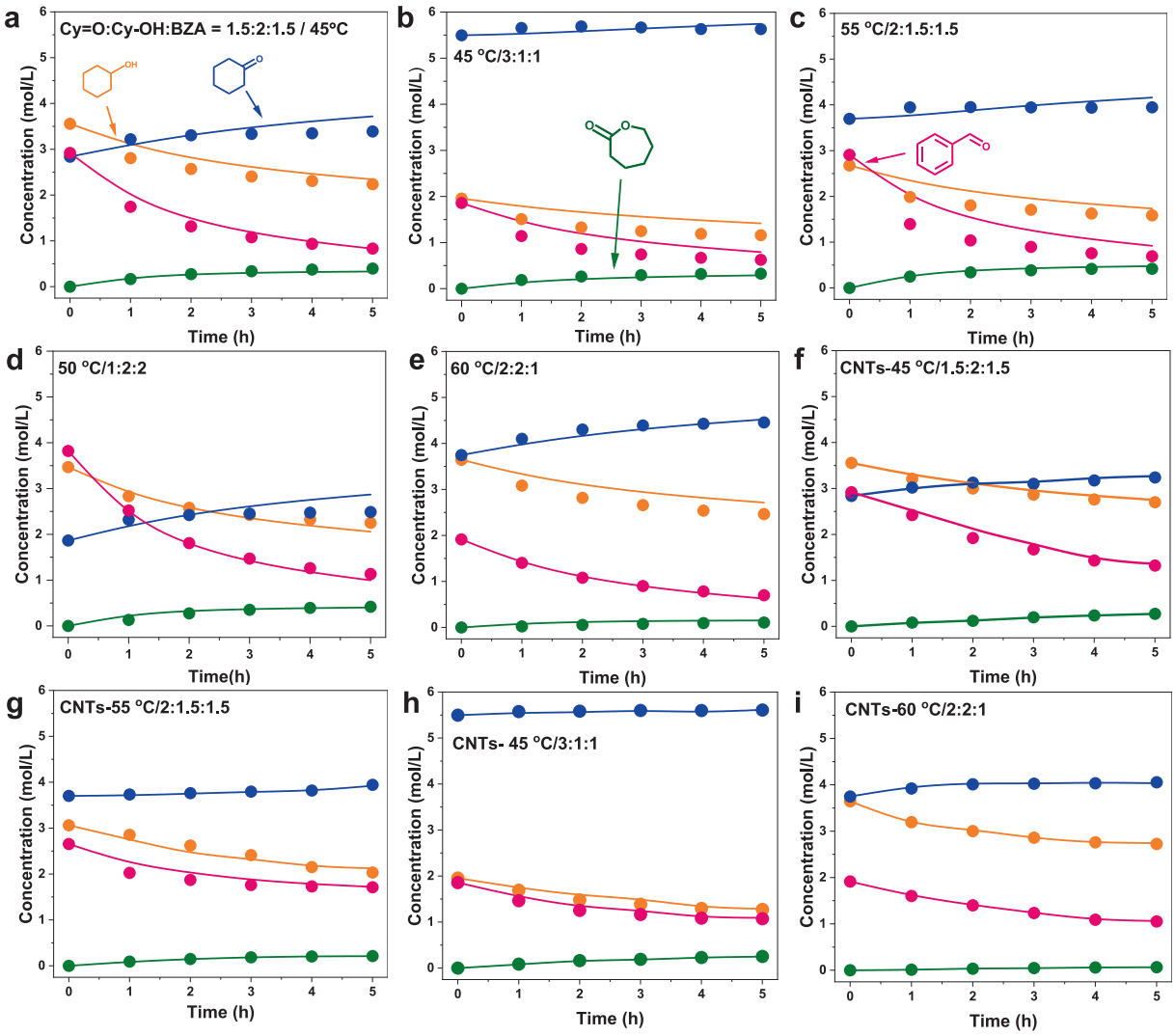

Fig. 5. Comparisons between the experimental (dots) and regressed (lines) data over different reaction conditions catalyzed by NCNTs (a-e) and CNTs (f-i) (conditions: 12 mg catalyst, 1100 rpm, 60 mL min^{-1} O_2).

confirmed that N doping significantly reduced the energy barrier of the oxidation reactions and accelerated the overall reaction rate. Notably, the activation energy for the autoxidation of BZA was relatively high, reaching 63.14 kJ·mol^{-1} on NCNTs and 86.88 kJ·mol^{-1} on CNTs, suggesting that this step was strongly influenced by temperature. Therefore, lowering the reaction temperature was expected to enhance the value of AE by suppressing the BZA autoxidation.

To validate the reliability of the kinetic parameters, the coefficient of determination (ρ^2), F-test (F_c), and residual analysis (R^2) were evaluated (**Eqs. 9–11**):

$$\rho^2 = 1 - \frac{\sum_1^j (C_{e,i} - C_{c,i})^2}{\sum_1^p C_{e,i}^2} \tag{9}$$

$$F_c = \frac{[\sum_1^j C_{e,i}^2 - \sum_1^j (C_{e,i} - C_{c,i})^2]/P}{[\frac{\sum_1^j (C_{e,i} - C_{c,i})^2}{j-P}]} \tag{10}$$

$$R^2 = \frac{\sum_1^j (C_{e,i} - C_{ave,i})^2 - \sum_1^j (C_{e,i} - C_{c,i})^2}{\sum_1^j (C_{e,i} - C_{ave,i})^2} \tag{11}$$

Where P was the number of parameters, j was the number of experiments, $C_{e,\,i}$ was the experimental value of the reactant concentration, $C_{c,\,i}$ was the calculated value of the reactant concentration, and $C_{ave,\,i}$ was the average value of the experimental results.

In this study, the calculated ρ^2 was 0.9842, revealing a good agreement between the obtained model and the observed data. The calculated F_c was 14467.5578, significantly exceeding the critical $F_{0.05}$ value (19.16 under the current conditions), showing the reasonability of the established kinetic model. Furthermore, the value of R^2 yielded 0.9889, demonstrating high consistency between simulated and experimental data. Additionally, the parity plot comparing calculated versus observed concentrations further validated the rationality of the established kinetic model. All data points were distributed uniformly along both sides of the diagonal (Fig. S15), showing the remarkable agreement between model estimates and experimental measurements. This alignment confirmed the reliability of the optimized rate constants obtained through the numerical simulation.

To verify the feasibility of the established kinetic model in predicting the results of KA oil oxidation to ε-CL, this study further extended the model to different operational conditions. Experimental data were collected under varied ketone/alcohol/aldehyde ratios and reaction temperatures (Fig. 6 and Table S6). Comparison between model predictions and experimental results shows strong agreement, particularly in the evolution of the intermediate Cy=O concentration and the final ε-CL. The results demonstrated that the established kinetic model reliably captured the dynamic relationships among reactant consumption,

Table 4
Elementary steps and kinetic parameters of KA oil oxidation catalyzed by NCNTs and CNTs.

Elementary steps	k_{45} ($\times 10^{-2}$)[a]		Reaction orders				E_a (kJ mol^{-1})	
	CNTs	NCNTs	CNTs Cy-OH or Cy=O	BZA	NCNTs Cy-OH or Cy=O	BZA	CNTs	NCNTs
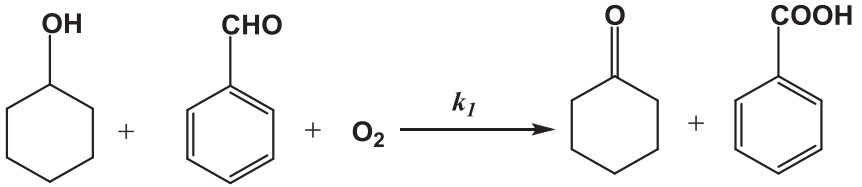	3.32	5	0.68	0.76	1.00	1.00	68.15	59.11
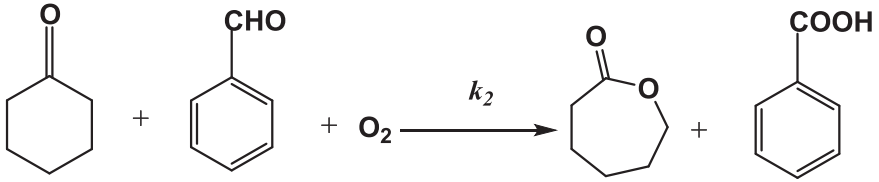	0.11	0.24	0.75	2.43	1.74	3.68	51.68	33.35
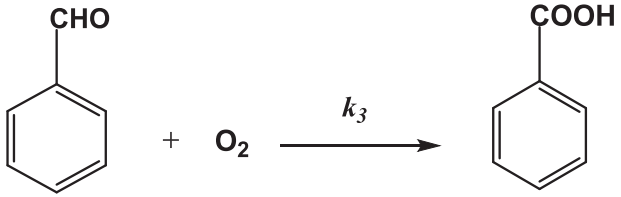	1.43	2	–	1.89	–	2.69	86.88	63.14

[a] The units of k_{45}: mol^{1-l-m} L^{-1-l-m} h^{-1}, mol^{-1-p-q} L^{-1-p-q} h^{-1}, mol^{1-n} L^{-1-n} h^{-1} for **SI, SII, SIII,** respectively.

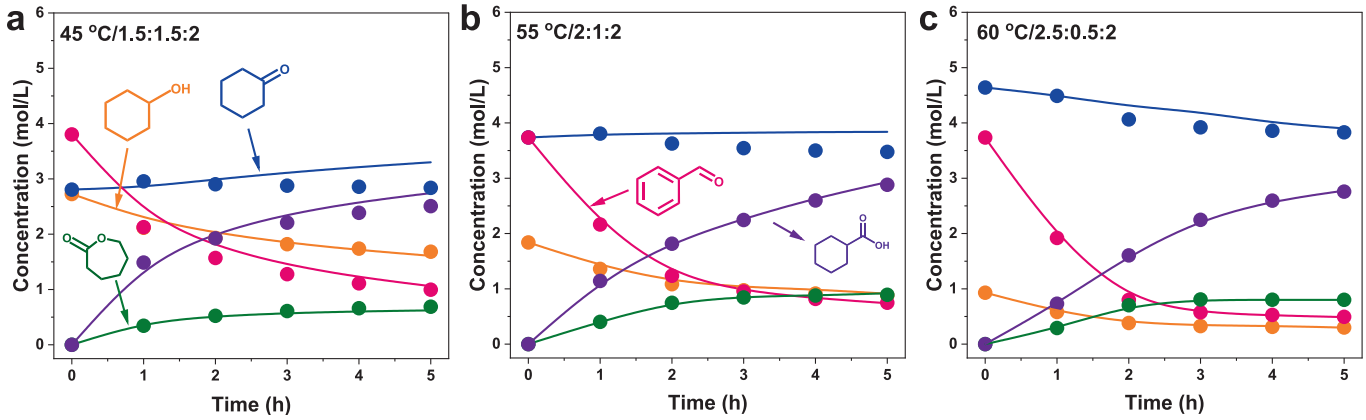

Fig. 6. Comparisons between the experimental (dots) and predicted (lines) data based on the obtained kinetic model over different reaction conditions catalyzed by NCNTs. Conditions: 12 mg catalyst, 1100 rpm, 60 mL min^{-1} O_2.

intermediate accumulation, and product formation under different feedstock compositions, confirming the feasibility of using the kinetic model to optimize process parameters for KA oil oxidation. Thus, this work provides a robust theoretical tool for mechanistic analysis and industrial condition prediction of complex multi-step oxidation reactions.

2.3. Process simulation and economic evaluation

Although laboratory-scale studies demonstrated promising catalytic performance, the industrial feasibility of the process remained to be fully evaluated. In this study, experimental investigation and process simulation were integrated to develop a continuous NCNT-catalyzed KA oil-to-ε-CL flowsheet using ASPEN Plus V17. Energy-integration optimization and a preliminary techno-economic analysis were subsequently performed to comprehensively assess the industrial potential and economic competitiveness of the technology.

Analysis of the composition and flow rates of the major streams in the converged flowsheet was essential for evaluating the rationality of the process design. As shown in Table S7, all key stream data reached steady

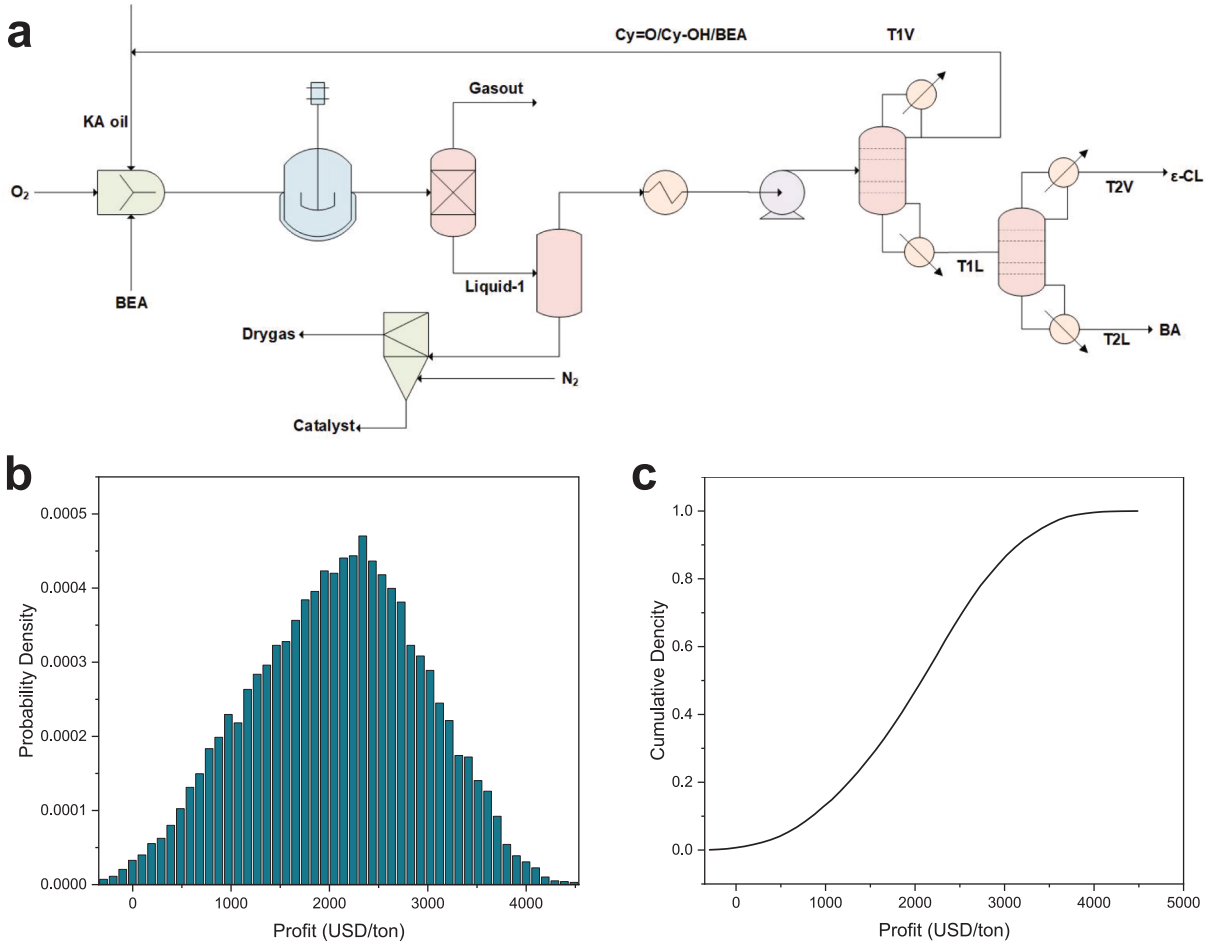

Fig. 7. (a) Flow diagram of the KA oil catalytic oxidation process. (b-c) The Monte Carlo analysis of the profit sensitivity.

state and satisfied the design specifications of each unit. The composition of the reactor effluent directly reflected catalytic performance. The ε-CL mole fraction of 97.3 % confirmed that the target product was successfully generated under the specified operating conditions. The efficiency of the separation system was demonstrated by comparing the compositions of the inlet and outlet streams. As illustrated in Fig. 7**a and S16**, the feed to the first distillation column was a complex reaction mixture. After two distillation stages, the product stream T2V achieved a ε-CL purity of 97.3 %, meeting industrial purity requirements and providing a qualified product basis for subsequent economic evaluation. The recycle stream T1V, composed primarily of unreacted KA oil with a total flow rate of 9.82 kmol h^{-1}, was returned to the reactor inlet. This increased the overall KA oil utilization from 44 % per pass to nearly 100 % and significantly reduced fresh feed consumption, serving as a key contributor to process economics. In summary, the stream-by-stream analysis confirmed that the developed flowsheet model not only successfully reproduced laboratory-scale catalytic results but also incorporated high-efficiency separation and recycle loops to achieve high-purity product recovery and near-quantitative raw-material reuse.

Building on the mass-balance data obtained from the steady-state flowsheet, a comprehensive techno-economic evaluation was performed to judge the industrial viability of the process. Energy duties, raw-material requirements and product revenues extracted from Aspen Plus were first consolidated in Table 5. On a basis, the utility demands were 0.8 kWh electricity, 4.7 *t* cooling water and 275.5 *t* steam to produce each *t* of ε-CL. When only feedstock and product credits were considered, excluding labour, maintenance, depreciation and other site costs, the cash cost of manufacturing one *t* of ε-CL was USD 4362.01. With a product value of USD 6529.25 t^{-1}, a pre-tax cash margin of USD 2167.23 t^{-1} was obtained, demonstrating that the catalytic route could generate ε-CL efficiently and profitably. The catalyst charge was orders of magnitude smaller than the substrate throughput, so its contribution to the cost sheet was negligible. Overall, the synthesis protocol met both technical and economic screens, and appeared attractive for scale-up.

Because profitability is sensitive to market volatility, a stochastic analysis was carried out to test the robustness of the cash margin. A Monte-Carlo simulation was chosen to quantify how simultaneous fluctuations in feed and product prices propagated into profit (Fig. 7**b and c**). One-year historical price series for KA oil, hydrogen, utilities and ε-CL were retrieved from public trading platforms; each variable was described by a triangular distribution whose mode corresponded to the median quotation and whose lower/upper bounds matched the observed minima and maxima (**Table S8**). Using NumPy's np.random.triangular, 10 000 price vectors were generated and the profit for each sample was computed. The resulting distribution was characterized by its mean, median, percentiles, and probability of loss (**Table S9**). The simulation returned an average profit of USD 2332.08 t^{-1} and a median of USD 2366.98 t^{-1}, the small difference indicating an almost symmetric distribution with a slight right skew. The worst-case scenario yielded a loss of USD 119.38 t^{-1}, illustrating that extreme feed-price spikes or product-price slumps could push the project into the red. Conversely, the best-case realization reached USD 4814.72 t^{-1}, highlighting substantial upside potential. The 30th percentile (P30) stood at USD 1 553.72 t^{-1}, meaning that in 90 % of the simulated futures the unit profit exceeded this threshold. Eighty per-cent of the outcomes fell between USD 858.58 t^{-1} and USD 3691.78 t^{-1}, confirming a consistently attractive return. Most importantly, the probability of a negative margin was only 0.95 %, and in 99.05 % of the cases the process remained profitable. Under the assumed price distributions the project therefore combined high expected returns with limited downside risk, reinforcing its industrial promise.

2.4. Life cycle assessment (LCA) analysis

A cradle-to-gate LCA was conducted to quantify the environmental footprint of the proposed reaction process, encompassing the extraction, manufacture, and consumption of feedstocks and energy (Huang et al., 2026; Sun et al., 2024) (Table 6). The analysis indicated that the primary environmental burdens of producing caprolactone from KA oil and BZA were concentrated in three categories: marine aquatic ecotoxicity potential (MAETP), global warming potential (GWP), and abiotic depletion of fossil resources (ADP-fossil). Specifically, MAETP constituted the dominant impact at 557,596.85 kg DCB-eq. Furthermore, the GWP reached 8,954.84 kg CO_2-eq, and the ADP-fossil amounted to 172,026.48 MJ, indicating substantial carbon emissions and fossil energy dependency.

In contrast, other environmental impact categories were relatively marginal. Human toxicity potential (HTP), freshwater aquatic ecotoxicity potential (FAETP), and terrestrial ecotoxicity potential (TETP) were limited to 587.02, 62.28, and 5.73 kg DCB-eq, respectively. Additional minor impacts included abiotic depletion of elements (0.00080 kg Sb-eq), acidification potential (18.91 kg SO_2-eq), photochemical ozone creation potential (3.09 kg ethene-eq), and eutrophication potential (2.13 kg PO_4^{3-}-eq), while ozone depletion potential (ODP) was practically zero.

A contribution analysis revealed that the generation of purchased electricity was the predominant source of the major environmental impacts, rendering all other material contributions negligible. Despite the footprint of external electricity, the proposed process inherently mitigated broader environmental burdens through key process engineering features. The direct utilization of KA oil circumvented the energy-intensive purification of Cy=O. Additionally, the solvent-free operation substantially curtailed the material and energy demands associated with solvent recovery, and the deployment of the highly active NCNT catalyst allowed for mild operating conditions, thereby minimizing overall thermal energy requirements.

3. Conclusion

In summary, this study demonstrates that NCNTs serve as an

Table 5
The consumption, costs and benefits obtained through process simulation calculations.

		Molar mass (kg $kmol^{-1}$)	Input (kmol h^{-1})	Mass (t h^{-1})	Consumption (ton/h or kWh h^{-1})	Unit price (USD t^{-1})	Sub (USD)
INPUT	Cy=O	98.14	12	1.18	0.83	12196.23	1012.22
	Cy-OH	100.16	6	0.6	0.15	13793.12	206.86
	BZA	106.12	12	1.28	1.21	20967.54	2537.14
	O_2	32	20	6.4×10^{-4}	6.4×10^{-4}	1377.42	0.09
	NCNTs	12	0.06	7.2×10^{-4}	7.2×10^{-4}	140,000	10.08
	Electricity	–	–	–	14.60	0.80	1.17
	Water	–	–	–	439	4.70	200.65
	Steam	–	–	–	14.30	275.50	393.97
	In total	–	–	–	–	–	4362.01
OUTPUT	ε-CL	114.14	9.48	1.08	1.08	49586.82	5355.44
	BA	74.08	10.53	0.78	0.78	15048.43	1173.84
	In total	–	–	–	–	–	6529.25
Profits	–	–	–	–	–	–	2167.23

Table 6
LCA parameter values of this reaction system.

Impact categories	Value (CML2001)[a]										
	GWP emission (kg CO_2 eq.)	ADP(f) (MJ)	HTP (kg DCB eq.)	TETP (kg DCB eq.)	ADP elements (kg Sb eq.)	POCP (kg C_2H_4 eq.)	ODP (kg R11 eq.)	AP (kg SO_2 eq.)	EP (kg Phosphate eq.)	FAETP (kg DCB eq.)	MAETP (kg DCB eq.)
Characteristic total value	8,954.84	172,026.48	587.02	5.73	0.00080	3.09	7.17×10^{-9}	18.91	2.13	62.28	557,596.85
Normalized value	83,240.55	1,204,185.38	4,167.84	38.93	0.00512	20.07	4.45×10^{-8}	115.32	14.08	423.52	3,791,658.59

[a] GWP: Global warming potential. ADP(f): Abiotic depletion potential such as coal, oil and natural gas. HTP: Human toxicity potential. TETP: Terrestric ecotoxicity potential. ADP: Abiotic depletion potential such as the consumption of mineral resources. POCP: Photochem ozone creation potential. ODP: Ozone layer depletion potential. AP: Acidification potential. EP: Eutrophication potential. FAETP: Freshwater aquatic ecotoxicity. MAETP: Marine aquatic ecotoxicity. DCB: 1,4-Dichlorobenzene. R11: Trichlorofluoromethane. Based on different environmental impact indicators, the contribution of different substances to the same environmental impact has been translated into harmonized baseline units.

effective catalyst for the oxidation of KA oil to ε-CL under mild conditions, achieving 19.68 % KA oil conversion and 39.12 % Cy-OH conversion with an atomic economy (AE) of 0.37, high STY (41.93 $g{\cdot}L^{-1}{\cdot}h^{-1}$), and low E-factor (2.76), which were much better than those of CNTs. Further analysis revealed a synergistic effect between N_P and N_G species in enhancing catalytic activity, which was confirmed by DFT simulations. While, the introduction of oxygen functional groups on the surface of carbon catalysts showed the negative effect on the ε-CL yield, but contributed to improve AE. The K/A ratios of CNTs and NCNTs were 1.54 and 2.00, respectively, demonstrating that N doping would enhance the transformation of Cy-OH toward ε-CL. Mechanism and kinetic studies suggested that N doping facilitated the generation and transfer of radical species, which played a critical role in the reaction network. NCNTs could promoted the initial oxidation of Cy-OH to Cy=O, which subsequently reacted with BZA to form ε-CL, thereby enhancing the overall reaction efficiency. N doping also would significantly lower the activation energies of all elementary steps compared to the CNT-catalyzed system. Process simulation results showed that the purity of all separated streams exceeds 99.5 %, validating the rationality of the proposed process design. Economic analysis indicates a profit range of approximately 858.58 to 3,691.78 USD per ton of ε-CL, suggesting favorable economic returns under most scenarios. LAC analysis revealed that the solvent-free reaction system catalyzed by NCNTs with KA oil as raw materials would lower the energy requirements This work not only advances the understanding of the NCNT-catalyzed KA oil oxidation but also proposes a cost-effective and scalable strategy for synthesizing biodegradable polymers, aligning with global initiatives in green chemistry and circular economy principles.

CRediT authorship contribution statement

Zhangzhi Li: Writing – original draft, Investigation, Data curation. **Yelin Guan:** Methodology, Investigation, Data curation. **Zhihui Cai:** Methodology, Investigation. **JieFeng Zhou:** Software, Investigation. **Hongjuan Wang:** Resources, Methodology. **Hao-Fan Wang:** Resources, Methodology. **Shuang Li:** Resources, Methodology. **Yonghai Cao:** Writing – review & editing, Supervision, Project administration, Funding acquisition. **Hao Yu:** Resources, Methodology.

Declaration of competing interest

The authors declare that they have no known competing financial interests or personal relationships that could have appeared to influence the work reported in this paper.

Acknowledgements

We would like to acknowledge the financial support from the National Natural Science Foundation of China (22272056), Guangdong Basic and Applied Basic Research Foundation (2026A1515010721) and CNPC Innovation Found (2021DQ02-0704).

Appendix A. Supplementary data

The experimental section such as chemical reagents, characterizations, DFT simulations, and LCA methodology can be found in the Supporting Information. Supplementary data to this article can be found online at https://doi.org/10.1016/j.ces.2026.123910.

Data availability

Data will be made available on request.

References

Bellomi, S., Barlocco, I., Tumiati, S., Fumagalli, P., Dimitratos, N., Roldan, A., Villa, A., 2023. Effects of oxygen functionalities on hydrous hydrazine decomposition over carbonaceous materials. Dalton Trans. 52 (43), 15871–15877.
Cai, Z., Liu, D., Huang, J., Feng, J., Wang, H., Yang, G., Peng, F., Cao, Y., Yu, H., 2022. Solvent-free production of ε-caprolactone from oxidation of cyclohexanone catalyzed by nitrogen-doped carbon nanotubes. Ind. Eng. Chem. Res. 61 (5), 2037–2044.
Cai, Z., Yuan, M., Wang, H., Wang, H.-F., Li, S., Cao, Y., Yu, H., Peng, F., 2025. Elucidating the influence of N doping on production of ε-caprolactone catalyzed by nanocarbon: a kinetic model from batch to semibatch and continuous-flow operations. Ind. Eng. Chem. Res. 64 (9), 4845–4857.
Cao, Y., Mao, S., Li, M., Chen, Y., Wang, Y., 2017. Metal/porous carbon composites for heterogeneous catalysis: Old catalysts with improved performance promoted by N-doping. ACS Catal. 7 (12), 8090–8112.
Cao, Y., Yu, H., Peng, F., Wang, H., 2014. Selective allylic oxidation of cyclohexene catalyzed by nitrogen-doped carbon nanotubes. ACS Catal. 4, 1617–1625.
Chen, G.W., Yuan, B., Wang, R.L., Yang, M., Wang, Z.K., Zhang, G.X., 2025. NHPI catalyzed air oxidation of cyclohexanone: Mechanism and kinetics study. Can. J. Chem. Eng. 103 (10), 5028–5038.
Chen, Z., Higgins, D., Chen, Z., 2010. Nitrogen doped carbon nanotubes and their impact on the oxygen reduction reaction in fuel cells. Carbon 48 (11), 3057–3065.
Chi, Y., Zhu, M., Li, Y., Yu, H., Wang, H., Peng, F., 2016. The effect of surface oxygenated groups of carbon nanotubes on liquid phase catalytic oxidation of cumene. Catal. Sci. Tech. 6 (7), 2396–2402.
Chizari, K., Janowska, I., Houllé, M., Florea, I., Ersen, O., Romero, T., Bernhardt, P., Ledoux, M.J., Pham-Huu, C., 2010. Tuning of nitrogen-doped carbon nanotubes as catalyst support for liquid-phase reaction. Appl. Catal. A 380 (1–2), 72–80.
Deng, J., Li, Y., Cao, Y., Wang, H., Yu, H., Zhang, Q., Zuo, J., Peng, F., 2020. Trace amounts of $Cu(OAc)_2$ boost the efficiency of cumene oxidation catalyzed by carbon nanotubes washed with HCl. Catal. Sci. Tech. 10 (8), 2523–2530.
Deng, Y., Chen, Z., Huang, J., Yang, G., Zhang, Q., Liu, Z., Cao, Y., Peng, F., 2022. MnO2 nanoparticles supported on CNTs for cumene oxidation: Synergistic effect and kinetic modelling. Chem. Eng. J. 444, 136666.
Du, R., Yuan, H., Yao, J., Li, H., 2019. Oxidation of KA oil to caprolactone with molecular oxygen using N-hydroxyphthalimide-mediated Ce(NH4)2(NO3)6 catalyst. Mol. Catal. 467, 24–29.
Fang, F., Dai, X., Peng, X., Sun, D., 2024. Baeyer-Villiger oxidation of cyclohexanone catalyzed by bifunctional Mg2Fe layered double hydroxide. Tetrahedron 164, 134165.
Fu, H., Huang, K., Yang, G., Cao, Y., Wang, H., Peng, F., Wang, Q., Yu, H., 2020. Synergistic effect of nitrogen dopants on carbon nanotubes on the catalytic selective epoxidation of styrene. ACS Catal. 10 (1), 129–137.

Gong, K., Du, F., Xia, Z., Durstock, M., Dai, L., 2009. Nitrogen-doped carbon nanotube arrays with high electrocatalytic activity for oxygen reduction. Science 323 (5915), 760–764.
Gross, R.A., Kalra, B., 2002. Biodegradable polymers for the environment. Science 297 (5582), 803–807.
Hu, Q., Huang, J., Wang, H., Yang, S., Wang, H.-F., Li, S., Cao, Y., Yu, H., 2025. Machine learning-driven kinetic elucidation for sustainable solvent-free continuous ε-caprolactone production via propionaldehyde-mediated nanocarbon catalysis. Ind. Eng. Chem. Res. 64 (31), 15296–15310.
Huang, J., Bai, J., Feng, J., Jiang, Q., Yang, G., Wang, H., Yu, H., Zhang, Q., Cao, Y., Peng, F., 2022. Catalytic synthesis of lactones from alkanes in the presence of aldehydes and carbon nanotubes. ACS Sustain. Chem. Eng. 10 (20), 6713–6723.
Huang, J., Chai, C., Wang, H., Wang, H.-F., Li, S., Yu, H., Cao, Y., 2026. Catalytic baeyer-villiger oxidation over N-doped carbon with aliphatic aldehyde: Mechanism, kinetic modeling, life cycle assessment, and techno-economic analysis. Chem. Eng. Sci. 320, 122666.
Jiménez-Sanchidrián, C., Ruiz, J.R., 2008. The Baeyer–Villiger reaction on heterogeneous catalysts. Tetrahedron 64 (9), 2011–2026.
Kim, J.-H., Hwang, S.Y., Park, J.E., Lee, G.B., Kim, H., Kim, S., Hong, B.U., 2019. Impact of the oxygen functional group of nitric acid-treated activated carbon on KOH activation reaction. Carbon. Lett. 29 (3), 281–287.
Li, Y., Guo, M., Yin, S., Chen, L., Zhou, Y., Qiu, R., Au, C., 2013. Graphite as a highly efficient and stable catalyst for the production of lactones. Carbon 55, 269–275.
Ma, X., Li, B., Shi, K., Liao, X., Wang, H., Tang, L., Zhang, L., Sun, Y., Li, J., 2021. Ni-Zn supported defective carbon with multi-functional catalytic sites for Baeyer–Villiger reaction using air as oxidant. J. Mater. Sci. 56 (26), 14684–14699.
Markowicz, F., Król, G., Szymańska-Pulikowska, A., 2019. Divergent effects of glucose and fructose on hepatic lipogenesis and insulin signaling. Ecol. Eng. 20 (1), 228–237.
Moudjahed, M., Dermeche, L., Idrissou, Y., Mazari, T., Rabia, C., 2022. Oxidation of cyclohexanone and/or cyclohexanol catalyzed by Dawson-type polyoxometalates using hydrogen peroxide. J. Chem. Sci. 134 (1), 31–41.
Mu, C., Cao, Y., Wang, H., Yu, H., Peng, F., 2018. A kinetics study on cumene oxidation catalyzed by carbon nanotubes: Effect of N-doping. Chem. Eng. Sci. 177, 391–398.
Nabae, Y., Rokubuichi, H., Mikuni, M., Kuang, Y.B., Hayakawa, T., Kakimoto, M., 2013. Catalysis by carbon materials for the aerobic baeyer-villiger oxidation in the presence of aldehydes. ACS Catal. 3 (2), 230–236.
Ning, X., Li, Y., Ming, J., Wang, Q., Wang, H., Cao, Y., Peng, F., Yang, Y., Yu, H., 2019. Electronic synergism of pyridinic- and graphitic-nitrogen on N-doped carbons for the oxygen reduction reaction. Chem. Sci. 10 (6), 1589–1596.
Shi, G., Kim, H., Koo, S., 2022. Oxo-carotenoids as efficient superoxide radical scavengers. Antioxidants (Basel) 11 (8), 1525.
Su, Y.Z., Huang, J.N., Yang, G.X., Wang, H.J., Yu, H., Zhang, Q., Cao, Y.H., Peng, F., 2023. Elucidating mechanism of ethylbenzene oxidation catalyzed by carbon-based catalysts with kinetic modeling. AIChE J 69 (5), e18007.
Sun, G., Cao, X., Wang, Y., Sun, X., Chen, Q., 2024. Comparative life cycle assessment of two different waste materials for recycled fiber. Resour. Conserv, Recycl, p. 205.
Sun, J., Gu, Q.Y., Jin, H.B., Yang, S.H., Qin, R., 2025. Fe-O-Sn Catalyst for ε-caprolactone synthesis: Kinetics and process optimization in B-V oxidation. Chem. Eng. Technol. 48 (9), e70108.
Tang, P., Hu, G., Li, M., Ma, D., 2016. Graphene-based metal-free catalysts for catalytic reactions in the liquid phase. ACS Catal. 6 (10), 6948–6958.
ten Brink, G.J., Arends, I.W., Sheldon, R.A., 2004. The Baeyer-Villiger reaction: new developments toward greener procedures. Chem. Rev. 104 (9), 4105–4124.
Tiwari, M.K., Jena, N.R., Mishra, P.C., 2018. Mechanisms of scavenging superoxide, hydroxyl, nitrogen dioxide and methoxy radicals by allicin: catalytic role of superoxide dismutase in scavenging superoxide radical. J. Chem. Sci. 130 (8).
Wang, J., Chen, X., Sim, L.B., Guan, L., He, X., Zhou, X., Chen, B., 2023. Unraveling the mechanism and kinetics of aerobic Baeyer Villiger oxidation of cyclohexanone. AIChE J 70 (1), e18263.
Wang, L., Li, B., Dionysiou, D.D., Chen, B., Yang, J., Li, J., 2022. Overlooked formation of H(2)O(2) during the hydroxyl radical-scavenging process when using alcohols as scavengers. Environ. Sci. Technol. 56 (6), 3386–3396.
Wang, Y., Chen, L., Chen, X., Yang, C., Cheng, X., Liu, W., Tiraferri, A., Ma, J., Liu, B., 2025. Overlooking the effect of alcohol quenchers can mislead mechanistic understanding in ferrate-based advanced oxidation processes. Sep. Purif. Technol. 370, 133193.
Wei, Q., Tong, X., Zhang, G., Qiao, J., Gong, Q., Sun, S., 2015. Nitrogen-doped carbon nanotube and graphene materials for oxygen reduction reactions. Catalysts 5 (3), 1574–1602.
Xue, G., Liu, H., Liu, W., Yang, C., Ban, Z., An, P., Chen, W., Zheng, L., Li, G., Tan, T., Tang, Z., 2024. Major-auxiliary cooperative metal pairs in MOFs enable cascade oxidation of KA oil to epsilon-caprolactone. Nat. Commun. 15 (1), 9659.
Yu, H., Peng, F., Tan, J., Hu, X., Wang, H., Yang, J., Zheng, W., 2011. Selective catalysis of the aerobic oxidation of cyclohexane in the liquid phase by carbon nanotubes. Angew. Chem. Int. Ed. 50 (17), 3978–3982.
Zhai, C., Li, S., Fan, Y., Tuo, J., Gong, X., Yang, T., Wan, Z., Ma, Y., Ma, Y., Wu, P., Xu, H., 2025. Anchoring Pd onto Sn sites in zeolite framework for baeyer–villiger oxidation with H2 and O2. ACS Catal. 15 (18), 15940–15949.
Zhang, C., Zheng, K., Ye, X., Yang, D., Zhou, L., Liang, K., Yun, J., 2025. Effects of nonmetallic heteroatoms doping on the catalytic performance of carbon materials. Chem. Eng. Sci. 304, 120980.
Zhang, Y., Zhao, Y., Jiang, W., Ya, Q., Li, Z., Gao, X., Liu, T., Yang, F., Wang, F., Liu, J., 2019. Lipase-catalyzed oxidation of cyclohexanone to form epsilon-caprolactone and kinetic modeling. ACS Sustain. Chem. Eng. 7 (15), 13294–13306.